Journal of Power Sources 242 (2013) 817–823

Contents lists available at SciVerse ScienceDirect

Journal of Power Sources

journal homepage: www.elsevier.com/locate/jpowsour

Formation of tungsten carbide nanoparticles on graphitized carbon to facilitate the oxygen reduction reaction

Zaoxue Yan [a,b], Guoqiang He [b], Mei Cai [c], Hui Meng [b], Pei Kang Shen [b,*]

[a] School of Chemistry and Chemical Engineering, Jiangsu University, Zhenjiang 212013, PR China
[b] State Key Laboratory of Optoelectronic Materials and Technologies, and Key Laboratory of Low-carbon Chemistry & Energy Conservation of Guangdong Province, School of Physics and Engineering, Sun Yat-sen University, Guangzhou 510275, PR China
[c] General Motors Research and Development Center, Warren, MI 48090-9055, USA

HIGHLIGHTS

- WC–graphite composite is synthesized through ion-exchange route.
- WC has controllable sizes between 2 and 10 nm.
- WC and graphite can be synthesized at low temperature of 750 °C.
- WC–graphite composite gives synergistic effect on Pt electrocatalyst.

ARTICLE INFO

Article history:
Received 20 April 2013
Received in revised form
21 May 2013
Accepted 29 May 2013
Available online 10 June 2013

Keywords:
Tungsten carbide
Platinum electrocatalyst
Oxygen reduction reaction
Synergistic effect
Ion-exchange route

ABSTRACT

Tungsten carbide nanoparticles with the average size less than 5 nm uniformly dispersed on the graphitized carbon matrix have been successfully synthesized by a one-step ion-exchange method. This route is to locally anchor the interested species based on an ionic level exchange process using ion-exchange resin. The advantage of this method is the size control of targeted nanomaterial as well as the graphitization of resin at low temperatures catalyzed by iron salt. The Pt nanoparticles coupled with tungsten carbide nanoparticles on graphitized carbon nanoarchitecture form a stable electrocatalyst (Pt/WC–GC). The typical Pt/WC–GC electrocatalyst gives a Pt-mass activity of 247.7 mA mg_{Pt}^{-1}, which is much higher than that of commercial Pt/C electrocatalyst (107.1 mA mg_{Pt}^{-1}) for oxygen reduction reaction due to the synergistic effect between Pt and WC. The presented method is simple and could be readily scaled up for mass production of the nanomaterials.

1. Introduction

Tungsten carbide (WC) has been found as a promoter that can enhance the catalytic activity of Pt, Pd and other alloy based electrocatalysts for alcohol oxidation, oxygen reduction reaction (ORR) and hydrogen evolution reaction due to the synergistic effect [1–14]. The kind of the electrocatalysts has the potential to reduce the noble metal usage while maintaining the same electrochemical performance, which will in turn reduce the cost of electrocatalysts. One of the key requirements to achieve the full synergistic effect is the atomic level mixture of the active components in an electrocatalyst, which requires the WC down to a single digit nanometer size. However, the WC particles prepared by previously reported methods [15] were generally larger than 20 nm with some particles size around 10 nm, synthesized by an intermittent microwave heating (IMH) method [16]. Although WC is stable in acidic media, the above WC particles are still too big and too heavy for the application in electrocatalyst.

It is a challenge to develop a novel method of synthesizing nanosized WC with a controllable size down to less than 5 nm. Pol et al. synthesized WC nanotubes with the diameter ranging from 30 to 70 nm [17,18]. Hu et al. prepared WC nanoparticles at an average size of 20 nm in diameter to support Pd nanoparticles which gave much better performance for ethanol oxidation than that of Pd/C electrocatalyst [19]. Zhu et al. prepared WC nanoparticles with the diameter of 10 nm on mesoporous carbon by carbothermal hydrogen reduction of chemisorbed phosphotungstic anions and found an enhanced thermal stability and good electrochemical stability for Pt supported electrocatalyst [9]. Wang et al. prepared WC nanoparticles with the size less than 10 nm by

* Corresponding author. Tel.: +86 20 84036736; fax: +86 20 84113369.
E-mail address: stsspk@mail.sysu.edu.cn (P.K. Shen).

0378-7753/$ – see front matter © 2013 Elsevier B.V. All rights reserved.
http://dx.doi.org/10.1016/j.jpowsour.2013.05.161

an in situ method [20]. The preparation of smaller WC nanoparticles below 10 nm in diameter is critical in order to enhance the synergistic effect of WC nanoparticles with noble metal nanoparticles.

Here, we report a one-step ion-exchange method of producing WC nanoparticles with controllable size ranging from 10 nm down to 2 nm on graphitized carbon. To the best of our knowledge, this is the first attempt in preparing such small WC nanoparticles directly onto graphitized carbon with a facile method.

2. Experimental

2.1. Synthesis of WC–GC (tungsten carbide–graphitized carbon composite)

A 100 ml aqueous solution of 50 mmol L^{-1} $K_4[Fe(CN)_6]$ (A.R., Guangzhou Chemical Reagent Co., China) mixed with ammonium metatungstate (AMT, A.R., Tianjin Jinke Fine Chemicals, China) at three concentrations of 14.3, 1.43 and 0.286 mmol L^{-1}, respectively and equally divided into 3 parts. The D314 polyacrylic weak-base anion exchange resin (10 g, Shanghai Hualing Resin Co., Ltd, China) was impregnated in the first part of the mixture for 2 h and then carefully washed with deionized water. The exchanged resin was impregnated again in the second and the third parts of the mixture following the same procedure and washed with deionized water. The exchanged resin was dried at 80 °C and then heated at 750 °C in N_2 atmosphere for 1 h to obtain WC–GC composite. The composite was grinded and treated in 5 mol L^{-1} HCl solution for 2 days to remove iron catalyst. The WC–GC with W precursor concentration of 14.3, 1.43 and 0.286 mmol L^{-1} were denoted as WC–GC9, WC–GC5 and WC–GC2, respectively. The corresponding average WC nanoparticle sizes were determined as 9.4 nm, 5.2 nm and 2.3 nm, respectively.

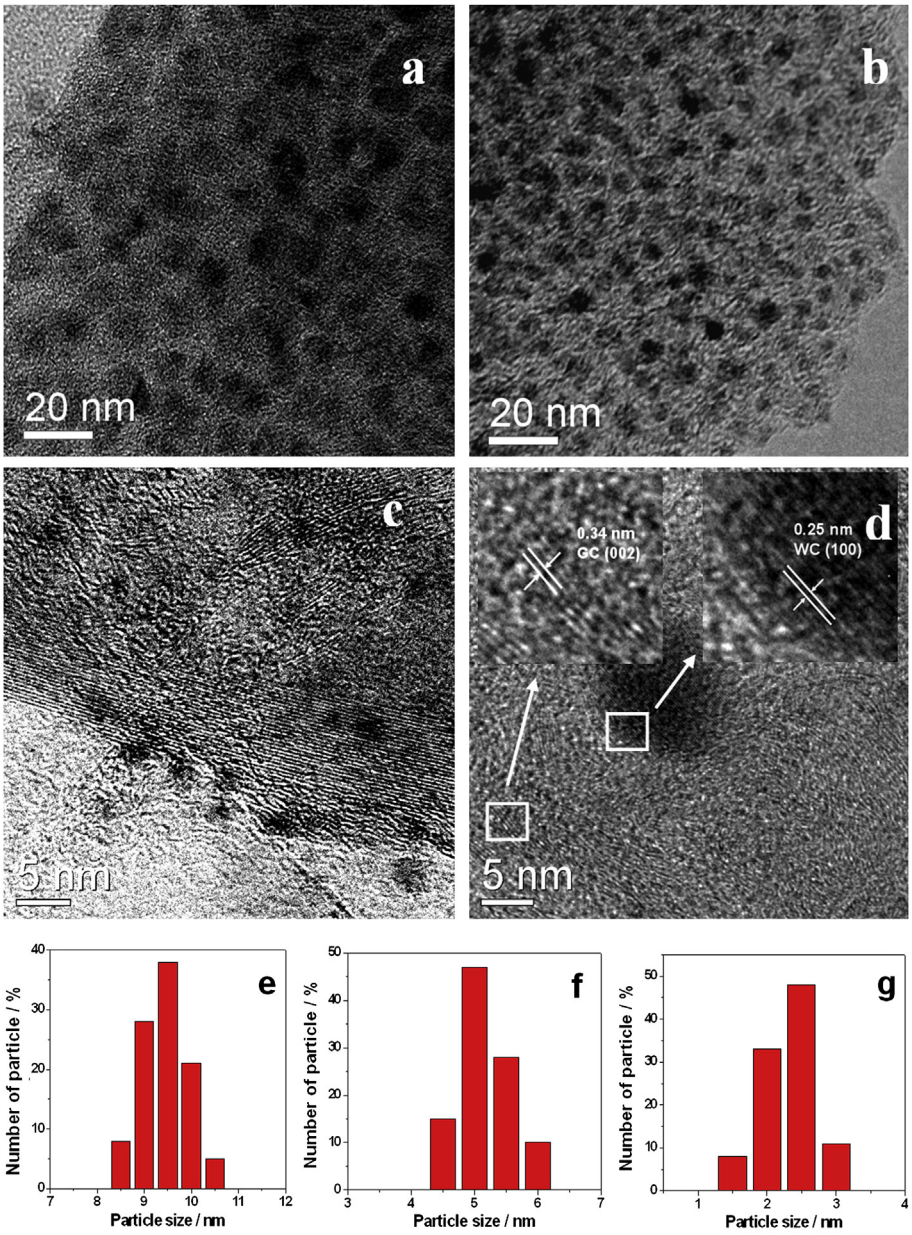

Fig. 1. The TEM images and the histograms of the materials. (a) WC–GC9, (b) WC–GC5, (c) WC–GC2 and (d) HRTEM image of WC–GC9. The WC particle size distribution of (e) WC–GC9, (f) WC–GC5 and (g) WC–GC2.

2.2. Preparation of electrocatalyst

Pt supported on the WC–GC9, WC–GC5 and WC–GC2 (denoted as Pt/WC–GC9, Pt/WC–GC5 and Pt/WC–GC2) was prepared. Typically, WC–GC (50 mg) was added into a mixture of 45.46 mg H_2PtCl_4 and 20 ml glycol (A.R., Tianjin Fuyu Fine Chemicals Co., Ltd, China) with sonication to form a uniform ink in an ultrasonic bath for 30 min. The pH of the mixture was then adjusted to 10 using 5 wt% NaOH/glycol solution (A.R., Guangzhou Chemical Reagent Factory, China). The sample was then placed into a homemade program-controlled microwave oven (1000 W, 2.45 GHz) for heating treatment with a 5 s on and 5 s off procedure for 20 times [21]. The product was finally washed for 5 times and dried in vacuum at 80 °C for 2 h. The Pt content in the electrocatalysts was targeted at 40 wt% stoichiometrically. The actual Pt contents were determined by inductively coupled plasma-atomic emission spectrometry (ICP, IRIS(HR), USA).

2.3. Characterization of electrocatalysts

Pt/WC–GC (5 mg) or commercial Pt/C (4 mg, 47.6 wt%Pt, TKK, Japan) was dispersed in mixed solution with 1.95 ml ethanol and 0.5 ml 0.5 wt% Nafion suspension (DuPont, USA) under ultrasonic agitation to form the electrocatalyst ink. The electrocatalyst ink (2.5 μl) was deposited on the surface of a rotating GC disk electrode and dried at room temperature. The total Pt loadings were maintained at 10 μg cm^{-2}. The electrochemical measurements were carried out in an oxygen-saturated 0.1 mol L^{-1} $HClO_4$ (A.R., Guangdong Guanghua Chemical Co., Ltd) solution scanned between 0 and 1.1 V vs. RHE at a scan rate of 5 mV s^{-1} at 25 °C. A platinum foil (1.0 cm^2) and a reversible hydrogen electrode (RHE) were used as counter and reference electrodes, respectively.

All chemicals were of analytical grade and used as received.

2.4. Physical characterization

The morphologies of the WC–GC and electrocatalysts were characterized by transmission electron microscopy (TEM, JEM-2010HR, JEOL Ltd., Japan) operating at 200 kV. The structures of the samples were determined on an X-ray diffractometer (XRD, D/Max-IIIA, Rigaku Co., Japan, CuK1, $\lambda = 1.54056$ Å radiation). The graphitization degree of WC–GC was determined by Laser Micro-Raman Spectrometer (Renishaw inVia, Renishaw plc, UK). The mass and heat change with temperature and time were determined by a thermogravimetry coupled with Fourier transform infrared spectrometry (TG-IR, TG-209/Vector-22, Germany Netzsch/Bruke Co.).

3. Results and discussion

Fig. 1 shows the TEM images of the nanosized WC on graphitized carbon. The WC–GC9, WC–GC5 and WC–GC2 represent different sizes of the WC samples. Fig. 1a shows the TEM image of the WC–GC9 sample prepared at higher concentration of AMT. The distribution of the WC nanoparticles is uniform, but, the average particle size is larger that is 9.4 nm in diameter (Fig. 1e). Fig. 1b indicates that the sample prepared at medium concentration of AMT (WC–GC5) yields much smaller WC size with better dispersion and distribution. The average particle size from a group of randomly selected particles is 5.2 nm (Fig. 1f). Even smaller WC particles could be prepared when lower AMT concentration was used in the synthesis. Typically, we have prepared WC nanoparticles with an average size of 2.3 nm (WC–GC2), as shown in Fig. 1c and g. The results demonstrated that the particle distribution of the WC is very

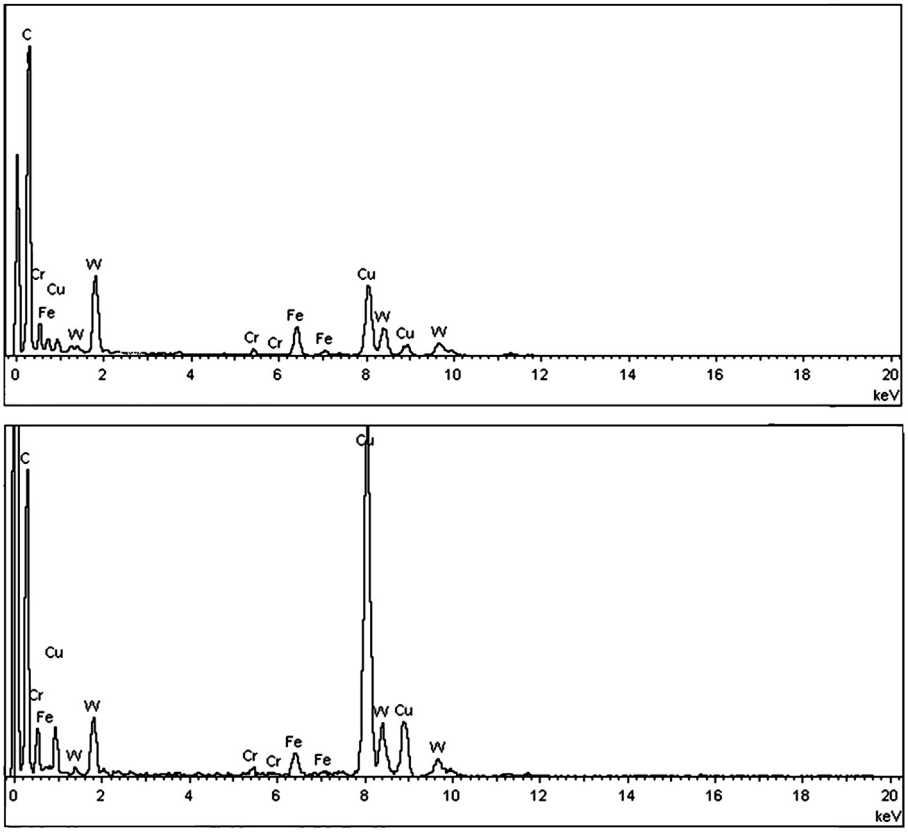

Fig. 2. The EDX patterns of WC–GC5 (up one) and WC–GC2 (down one).

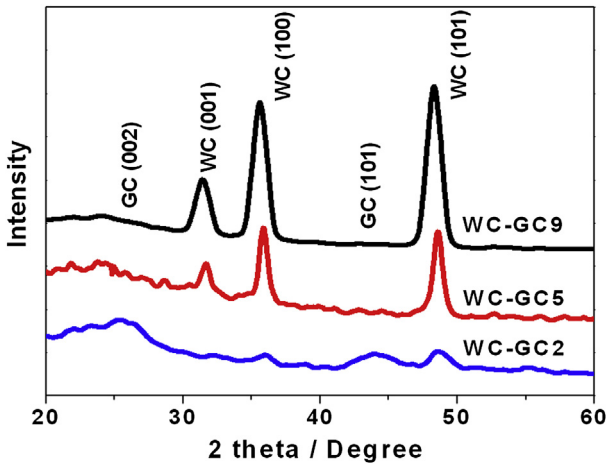

Fig. 3. XRD patterns of WC–GC9, WC–GC5 and WC–GC2.

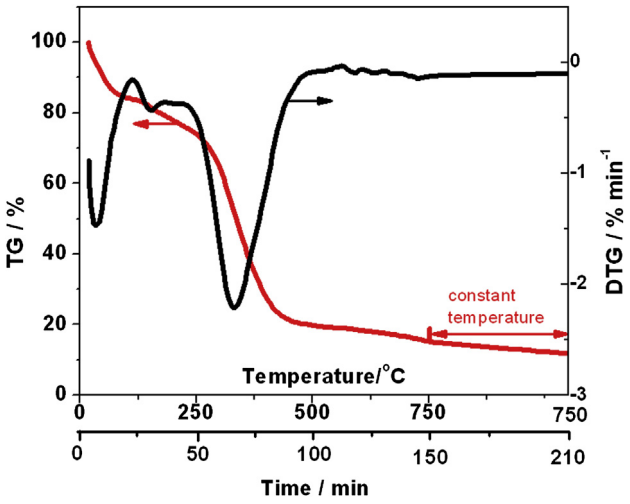

Fig. 5. TG and DTG results of the sample after ion exchanged in medium AMT concentration in N_2 atmosphere at the heating rate of 5 °C min^{-1}.

uniform by the ion exchange method. Fig. 1d is the high resolution transmission electron microscopic (HRTEM) image of WC–GC5. It clearly shows the crystalline lattices of WC (100) and GC (002) facets, which reveals that this resin can be graphitized at 750 °C by iron catalyst along with the formation of WC. We have repeated the experiments many times and have confirmed the formation of WC at such a low temperature.

The EDS patterns of WC–GC5 and WC–GC2 are shown in Fig. 2, which indicate the existence of W and C elements. The peaks corresponding to Fe element (catalyst for low temperature graphitization) were also found in Fig. 2.

Fig. 3 shows the XRD patterns of WC–GC9, WC–GC5 and WC–GC2 samples. The peaks at 31.5°, 35.6° and 48.3° correspond to the (001), (100) and (101) facets of WC crystal and the peaks at 26.4° and 44.4° correspond to the (002) and (101) facets of GC. The WC nanoparticles are getting smaller with weaker peak intensity when the lower concentration of AMT was used during the ion exchange process. Significantly, compared to the WC prepared by other methods [15,22–26] at the temperature over 1000 °C while metal W, W_2C and WO_3 co-existed, the WC nanoparticles prepared under the present conditions is pure WC without any impurities (Fig. 3). This method will be interested for energy-saving in the mass production of the nanosized metal carbides.

The Raman spectroscopic measurements shown in Fig. 4 indicate that the resin was partially graphitized with the iron catalyst. The ratios of the G-line to D-line in Fig. 4 were used to determine the degree of the graphitization. The G peak at 1584 cm^{-1} corresponds to a splitting of the E_{2g} stretching mode of graphite and reflects the structural intensity of the sp^2-hybridized carbon atom [27,28]. It also has a positive shift compared to that of the highly oriented pyrolytic graphite (HOPG, 1580 cm^{-1}). The D peak at 1350 cm^{-1} is attributed to the vibrations of carbon atoms with dangling bonds in disordered graphite planes and the defects incorporated into pentagon and heptagon graphite-like structures. The I_G/I_D values for WC–GC9, WC–GC5 and WC–GC2 are 1.19, 1.22 and 1.30, respectively. These results indicate that the samples prepared in dilute AMT concentration yield a higher degree of graphitization. This observation can be explained as follow: when the concentration of tungsten precursor was reduced while the concentration of iron precursor was maintained the same, the total number of exchanged iron would be higher, resulting a higher degree of graphitization.

Fig. 5 shows the TG and differential scanning calorimetry results of the sample, after ion exchange with medium AMT concentration,

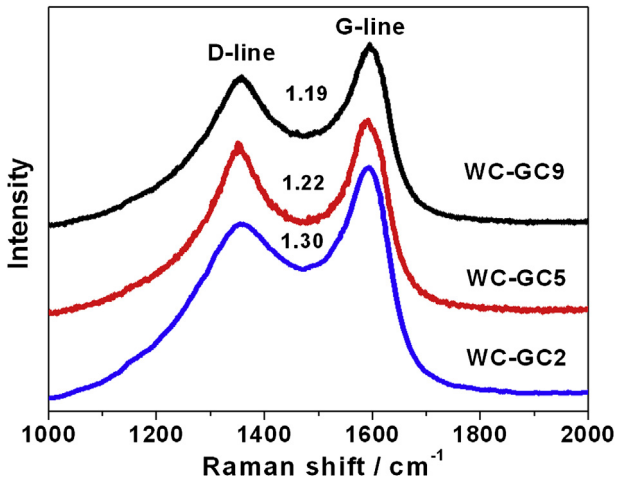

Fig. 4. The Raman spectra of the three WC on graphitized carbon samples.

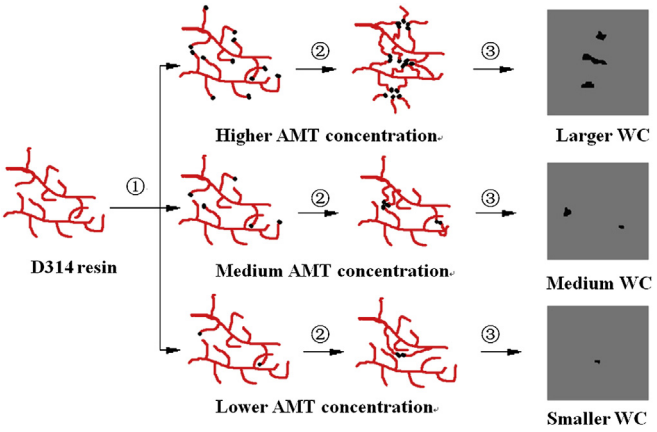

Fig. 6. Schematic synthesis process of WC nanoparticles at different diameters. Step ①: Pretreated D314 is exchanged by AMT at different concentrations; step ②: Tungsten precursor ions ($W_7O_{24}^{6-}$) tied on resin by ion exchange and collapsed to form larger WC nanoparticles during the heating process; step ③: WC nanoparticles at different particle size on graphitized carbon formed.

Table 1
Comparison of WC in samples of WC–GC9, WC–GC5 and WC–GC2.

Sample	Mass after heat treated (g)	Mass of WC (g)	Mass content of WC %	WC size (nm)
D314 (10 g)	1.22	/	/	/
D314 (10 g) + W (0.1 mol L^{-1} 100 ml)	3.02 (WC–GC9)	1.92	63.6	9.4
D314 (10 g) + W (0.01 mol L^{-1} 100 ml)	1.40 (WC–GC5)	0.19	13.6	5.2
D314 (10 g) + W (0.002 mol L^{-1} 100 ml)	1.25 (WC–GC2)	0.03	2.4	2.3

in N_2 atmosphere. The mass loss before 80 °C represents the evaporation of free water moisture. The sharp mass loss between 300 and 450 °C corresponds to the evaporation and decomposition of the resin with CO and CO_2 released from the sample. The slower mass loss after 500 °C corresponds to a continuous process of carbonization and graphitization of the melted resin along with the formation of WC nanoparticles. The DTG curve finally reached zero after 1 h at 750 °C, indicating the complete conversion of stable WC nanoparticles.

Fig. 6 illustrates the synthesis process of WC nanoparticles with different diameters, which also explains the influence of the AMT concentration on the WC size. In the first step, $W_7O_{24}^{6-}$ anions are locally attached onto the active sites of the resin through the ionic-level exchange of the $W_7O_{24}^{6-}$ anions with OH^- ions on D314 resin.

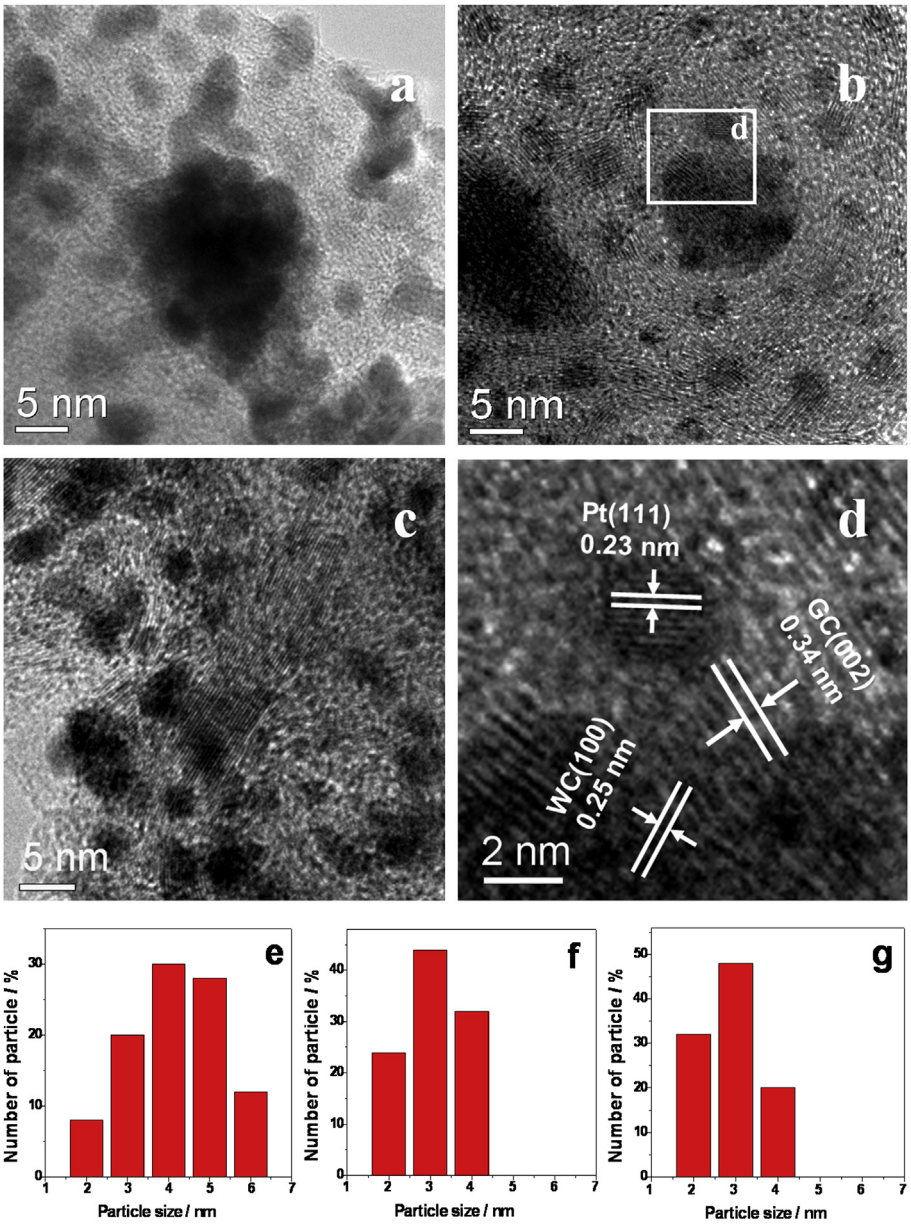

Fig. 7. TEM images of the materials. (a) Pt/WC–GC9, (b) Pt/WC–GC5, (c) Pt/WC–GC2 and (d) HRTEM image of Pt/WC–GC5. And the corresponding Pt particle size distributions in (e) Pt/WC–GC9, (f) Pt/WC–GC5 and (g) Pt/WC–GC2.

Table 2
The performance comparison of the four electrocatalysts.

Electrocatalyst	I_G/I_D	Pt mass content[a]	Pt particle size[b] (nm)	ECSA ($m^2\ g^{-1}$)	i_m at 0.9 V (mA mg_{Pt}^{-1})
Pt/WC–GC9	1.19	35.2%	4.1	31.1	117.2
Pt/WC–GC5	1.22	36.9%	3.1	37.9	247.7
Pt/WC–GC2	1.30	37.3%	2.9	39.5	136.2
Pt/C-TKK	–	47.6%	–	36.3	107.1

[a] The data were determined by inductively coupled plasma-atomic emission spectrometry (ICP).
[b] The data were calculated from Fig. 7.

The second step is the conversion of $W_7O_{24}^{6-}$ on D314 into WC nanoparticles by heat treatment. The concentration effect is most probably due to the conglomeration caused by more $W_7O_{24}^{6-}$ anions being exchanged, as shown in Fig. 6. The resin will then undergoes evaporation and decomposition processes followed by carbonization and graphitization process at higher temperatures. The resin structure finally collapses to form WC nanoparticles. Depending on the amount of the available tungsten precursor, the more the exchanged tungsten precursor, the larger the WC nanoparticle is. Table 1 summarized the data of the samples.

The as-synthesized WC–GC9, WC–GC5 and WC–GC2 were used as supporting substrates to produce Pt based electrocatalysts. Fig. 7a–c shows the TEM images of Pt loaded WC–GC including Pt/WC–GC9, Pt/WC–GC5 and Pt/WC–GC2. Fig. 7e–g shows the corresponding Pt particle distributions, and the average Pt particle sizes for each electrocatalyst are summarized in Table 2. It can be seen that the Pt nanoparticles on WC–GC5 and WC–GC2 have smaller sizes and narrower size distributions than that on WC–GC9, which should result from different specific surface areas of WC–GC matrices due to different WC mass content (Table 1). From the HRTEM image (Fig. 7d), the crystalline lattices of WC (100), Pt (111) and GC (002) facets can be clearly observed. The XRD patterns of Pt/WC–GC9, Pt/WC–GC5 and Pt/WC–GC2 are shown in Fig. 8. Besides the WC peaks, the peaks at 39.8°, 46.2°, and 67.5° correspond to the (111), (200) and (220) facets of Pt crystal respectively. This catalyst made with WC and Pt nanoparticles uniformly dispersed on graphitized carbon are expected to show better catalytic performance.

This electrocatalysts made with WC and Pt nanoparticles uniformly dispersed on graphitized carbon were further tested for ORR, which is critical to significant improving the performance of proton exchange membrane fuel cells [29–32]. Fig. 9a shows the linear polarization curves for ORR on Pt/WC–GC9, Pt/WC–GC5, Pt/WC–GC2 and commercial Pt/C electrodes in O_2 saturated 0.1 mol L^{-1} $HClO_4$ solution with a scan rate of 5 mV s^{-1} and rotating rate of 1600 r min^{-1} at 25 °C. By comparing the activity at 0.9 V, it is clear that the current density on Pt/WC–GC5 is much higher than the others. Fig. 9b shows the kinetic current of two electrocatalysts calculated from the experimental data using the well-known mass transport correction for rotating disk electrode [33]:

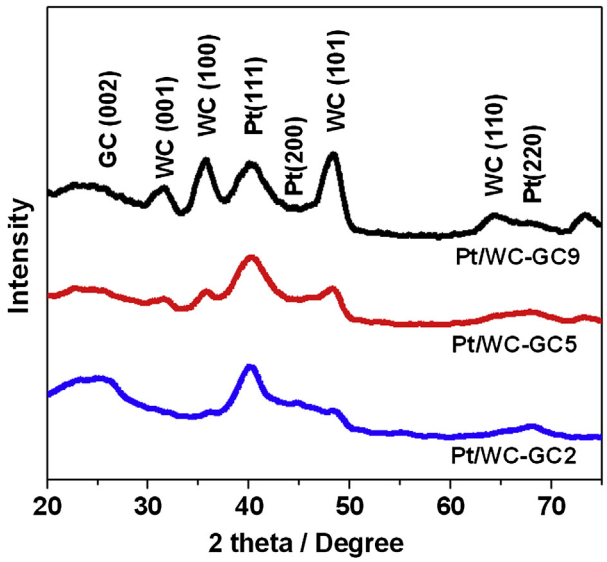

Fig. 8. XRD patterns of Pt/WC–GC9, Pt/WC–GC5 and Pt/WC–GC2.

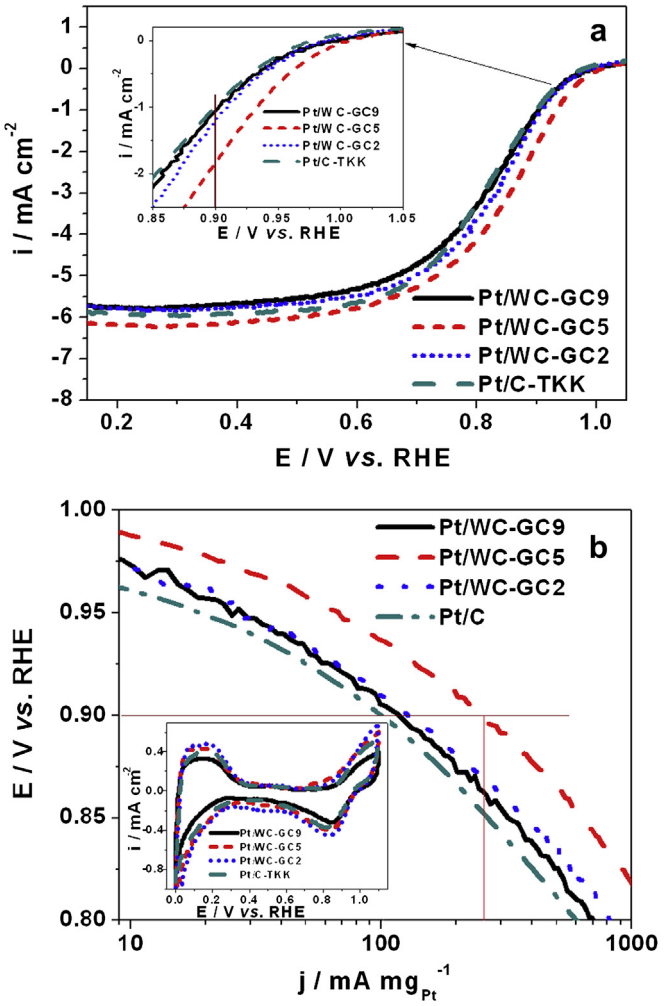

Fig. 9. The ORR performance. (a) ORR on Pt/WC–GC9, Pt/WC–GC5, Pt/WC–GC2 and Pt/C electrodes in O_2 saturated 0.1 mol L^{-1} $HClO_4$ solution, 25 °C, scan rate: 5 mV s^{-1}, 1600 r min^{-1}. The inset in (a) is the enlarged curves. (b) The corresponding mass activity–potential plots. The inset in (b) is the cyclic voltammograms of the four electrodes in 0.1 mol L^{-1} $HClO_4$ solution at 25 °C, scan rate: 50 mV s^{-1}.

$$i_k = i_d i/(i_d - i) \quad (1)$$

where i is the experimentally obtained current, i_d refers to the measured diffusion-limited current and i_k the mass-transport-free kinetic current. The mass activity can be determined via the calculation of i_k using Equation (1) and normalized with the Pt loadings. The Pt-mass activities, i_m, measured from the curves in Fig. 9b are summarized in Table 2. The inset in Fig. 8 is the cyclic voltammograms of the four electrodes in 0.1 mol L^{-1} $HClO_4$ solution at 25 °C, scan rate: 50 mV s^{-1}. The electrochemical surface area (ECSA) for each electrocatalyst is calculated (assuming that $Q_H = 210$ μC cm^{-2} for a smooth polycrystalline Pt [34,35]) and also summarized in Table 2. Among the three Pt/WC–GC electrocatalysts, Pt/WC–GC5 has the highest mass activity of 247.7 mA mg_{Pt}^{-1} for ORR. The reason why Pt/WC–GC9 showed lower ORR performance comparing to Pt/WC–GC5 is due to the larger size and amount of WC which has low efficiency of synergistic effect and low ECSA (see Table 2). As for WC–GC2, it has too low WC mass content (see Table 1), resulting in too weak synergistic effect on Pt, so the mass activity of Pt/WC–GC2 was lower than Pt/WC–GC5. In this study, the measured activity of a chosen commercial Pt/C electrocatalyst is in good agreement with the reported or predicted value in literature [33,36].

4. Conclusions

The composite of WC nanoparticles down to less than 5 nm on graphitized carbon was successfully synthesized through a novel route of locally attaching the interested species based on an ionic level exchange process using ion-exchange resin. The advantage of this method is the size control of targeted nanomaterial as well as the graphitization of resin at a temperature of 750 °C catalyzed by iron salt. The product consists of a Pt nanoparticles coupled with tungsten carbide nanoparticles on graphitized carbon nanoarchitecture to form a stable electrocatalyst. The Pt/WC–GC5 electrocatalyst gave a mass kinetic current of 247.7 mA mg_{Pt}^{-1}, which is much higher than that of commercial Pt/C electrocatalyst (107.1 mA mg_{Pt}^{-1}) for ORR. The method is simple and could be readily scaled up for mass production.

Acknowledgments

This work was supported by the National Natural Science Foundation of China (21073241, U1034003), the China National 863 Program (2009AA034400), the State Key Laboratory of Optoelectronic Materials and Technologies (2010-ZY-4-4, 2010-ZY-4-7) and General Motors (Project No. RD-07-295-NV508). Dr. Z.X. Yan thanks the support by China Postdoctoral Science Foundation (2012M521011). Dr. H. Meng thanks the New Teacher Funding of Sun Yat-sen University (30000-3126170).

References

[1] H. Chhina, S. Campbell, O. Kesler, J. Power Sources 179 (2008) 50–59.
[2] Y. Wang, S. Song, V. Maragou, P.K. Shen, P. Tsiakaras, Appl. Catal. 89 (2009) 223–228.
[3] I.J. Hsu, Y.C. Kimmel, Y. Dai, S. Chen, J.G. Chen, J. Power Sources 199 (2012) 46–52.
[4] F. Hu, G. Cui, Z. Wei, P.K. Shen, Electrochem. Commun. 10 (2008) 1303–1306.
[5] Z. Zhao, X. Fang, Y. Li, Y. Wang, P.K. Shen, F. Xie, X. Zhang, Electrochem. Commun. 11 (2009) 290–293.
[6] R. Ganesan, D.J. Ham, J.S. Lee, Electrochem. Commun. 9 (2007) 2576–2579.
[7] D.D. Vasić, I.A. Pašti, S.V. Mentus, Int. J. Hydrogen Energy 38 (2013) 5009–5018.
[8] X.B. Gong, S.J. You, X.H. Wang, Y. Gan, R.N. Zhang, N.Q. Ren, J. Power Sources 225 (2013) 330–337.
[9] Q. Zhu, S. Zhou, X. Wang, S. Dai, J. Power Sources 193 (2009) 495–500.
[10] H. Meng, P.K. Shen, Z.D. Wei, Electrochem. Solid-State Lett. 7 (2006) A368–A372.
[11] M. Wu, P.K. Shen, Z. Wei, S. Song, M. Nie, J. Power Sources 166 (2007) 310–316.
[12] S. Sharma, B.G. Pollet, J. Power Sources 208 (2012) 96–119.
[13] H. Binder, A. Köhling, W. Kuhn, W. Lindner, G. Sandstede, Nature 224 (1969) 1299–1300.
[14] J.P. Bosco, K. Sasaki, M. Sadakane, W. Ueda, J.G. Chen, Chem. Mater. 3 (2010) 966–973.
[15] S.R. Vallance, S. Kingman, D.H. Gregory, Adv. Mater. 19 (2007) 138–142.
[16] P.K. Shen, S. Yin, Z. Li, C. Chen, Electrochim. Acta 55 (2010) 7969–7974.
[17] V.G. Pol, S.V. Pol, A. Gedanken, Adv. Mater. 23 (2011) 1179–1190.
[18] S.V. Pol, V.G. Pol, A. Gedanken, Adv. Mater. 18 (2006) 2023–2027.
[19] F.P. Hu, P.K. Shen, J. Power Sources 173 (2007) 877–881.
[20] R. Wang, C. Tian, L. Wang, B. Wang, H. Zhang, H. Fu, Chem. Commun. (2009) 3104–3106.
[21] Z.Q. Tian, F.Y. Xie, P.K. Shen, J. Mater. Sci. 39 (2004) 1509–1511.
[22] T. Iizuka, H. Kita, H. Hyuga, T. Hirai, K. Osumi, J. Am. Ceram. Soc. 87 (2004) 337–341.
[23] J. Temuujin, M. Senna, T. Jadambaa, D. Byambasuren, J. Am. Ceram. Soc. 88 (2005) 983–985.
[24] M.H. Lin, Ceram. Int. 31 (2005) 1109–1115.
[25] R. Yang, T. Xing, R. Xu, M. Li, Int. J. Refract. Met. Hard Mater. 29 (2011) 138–140.
[26] D. Demirskyi, A. Ragulya, D. Agrawal, Ceram. Int. 37 (2011) 505–512.
[27] M.S. Dresselhaus, G. Dresselhaus, R. Saito, A. Jorio, Phys. Rep. 409 (2005) 47–99.
[28] T. Belin, F. Epron, Mater. Sci. Eng. B 119 (2005) 105–118.
[29] K. Gong, F. Du, Z. Xia, M. Durstock, L. Dai, Science 323 (2009) 760–764.
[30] J. Zhang, K. Sasaki, E. Sutter, R.R. Adzic, Science 315 (2007) 220–222.
[31] M. Lefèvre, E. Proietti, F. Jaouen, J.-P. Dodelet, Science 324 (2009) 71–74.
[32] D. Strmcnik, M. Escudero-Escribano, K. Kodama, V.R. Stamenkovic, A. Cuesta, N.M. Markovic, Nat. Chem. 2 (2010) 880–885.
[33] H.A. Gasteiger, S.S. Kocha, B. Sompalli, F.T. Wagner, Appl. Catal. B 56 (2005) 9–35.
[34] H.J. Kim, D.Y. Kim, H. Han, Y.G. Shul, J. Power Sources 159 (2006) 484–490.
[35] Z. Yan, H. Wang, M. Zhang, Z. Jiang, T. Jiang, J. Xie, Electrochim. Acta 95 (2013) 218–224.
[36] B. Lim, M.J. Jiang, P.H.C. Camargo, E.C. Cho, J. Tao, X.M. Lu, Y.M. Zhu, Y.A. Xia, Science 324 (2009) 1302–1305.